Indonesian Journal of Environmental Management and Sustainability
e-ISSN:2598-6279 *p*-ISSN:2598-6260

IJEMS

Research Paper

Utilization of Coffee Peel Waste as Biosorbent for Rhodamine B Dye Removal: Isotherm, Kinetics, and Thermodynamic Studies

Rahmiana Zein[1*], Yona Prestica[1], Deswati[1], Putri Ramadhani[2]

[1]*Department of Chemistry, Faculty of Mathematics and Natural Sciences, Andalas University, Padang, 25163, Indonesia*
[2]*Advanced Chemistry Research Center, National Research and Innovation Agency (BRIN), Tangerang Selatan, 15314, Indonesia*
***Corresponding author e-mail**: rzein@sci.unand.ac.id

Abstract
Coffee Peel Waste (CPW) is an abundant and inexpensive material that can be employed as a biosorbent to remove Rhodamine B (RB) dye from wastewater. This research utilized the batch adsorption approach to optimize the parameters of pH, starting concentration of dye and period of contact. At pH 8, 1000 mg/L as the starting concentration and 105 minutes as the contact time, the optimal conditions were established, exhibited an adsorption capacity of 71.8454 mg/g, aligning with the Langmuir isotherm model, wherein mechanism of adsorption demonstrated monolayer adsorption, and was most appropriate for the kinetic model of pseudo-second order. Thermodynamic analysis revealed that the adsorption occurred spontaneously and released heat, confirming its exothermic nature. FTIR characterization identified the functional sites involved in the adsorption mechanism. At the same time, SEM-EDX analysis showed morphological changes and an increase in some aspects after adsorption, confirming the attachment of RB to the surface of the CPW. This study reveals the advantages of CPW as an innovative, efficient and sustainable biosorbent, offering a new solution in wastewater treatment based on agro-industrial waste.

Keywords
Adsorption, Coffee Peel Waste, Isotherm, Kinetics, Rhodamine B

Received: 20 December 2024, Accepted: 15 March 2025
https://doi.org/10.26554/ijems.2025.9.1.36-45

1. INTRODUCTION

The use of synthetic dyes is prevalent across diverse industries. However, their extensive use generates wastewater that harms human health and the environment (Cheruiyot et al., 2019). RB is among the most commonly used synthetic dyes, particularly in pens, carbon sheets, paints, leather, stamp ink, and fireworks (Amalina et al., 2022). Its non-biodegradable nature permits it to survive for long periods of time in water, worsening its ecological impact (Al-Kahtani, 2017). It is toxic to aquatic organisms, disrupts the photosynthesis process in aquatic organisms, and labeled as a possible carcinogen by IARC (International Agency for Research on Cancer, 2022; Palapa et al., 2023). Long-term exposure has been tied to dermal irritation, respiratory disorders, and liver and kidney damage (Al-Tohamy et al., 2022).

Various physicochemical strategies have been devised to eliminate synthetic dyes from wastewater. However, adsorption is preferred due to its excellent effectiveness, inexpensive, minimal chemical use, and ease of application (Harrache et al., 2019; Subramaniam and Kumar Ponnusamy, 2015). Agricultural waste is increasingly explored as an adsorbent because of its abundance, high carbon content (cellulose, lignin, hemicellulose), and adsorption ability. Agricultural waste also has suitable chemical and physical properties without complex processing (Rangabhashiyam et al., 2013). Extensive research has utilized agricultural waste as RB biosorbents, such as garlic peels with an uptake capacity of 3.5 mg/g Zhao et al. (2019), pomegranate peels 30.47 mg/g Ghibate et al. (2021), pine cones 6.83 mg/g Gul et al. (2022)), and almond shells 14.7 mg/g (Senol et al., 2023).

Coffee peel is another promising agricultural waste-based biosorbent. Its chemical composition is listed in Table 1 (Dung et al., 2023). The primary components, which include hemicellulose, cellulose, and lignin, contain functional groups like carbonyl (C=O) and hydroxyl (−OH), enabling the adsorption of pollutants. Indonesia, holding the position of the ranked world's third most prolific coffee producer, trailing Brazil and Vietnam, continues to increase its coffee production. The Central Statistics Agency (BPS) it was documented that Indonesia's coffee output in 2022 reached approximately 794.8 thousand tons, reflecting a growth of

around 1.1% compared to the preceding year. However, most CPW remains underutilized, often discarded as animal feed, burned, or dumped into rivers, causing environmental issues. Its high water content (75–80%) creates unpleasant odours (Juwita et al., 2017). Therefore, this research examines the viability of CPW as a sustainable and environmentally responsible adsorbent for RB removal while promoting its beneficial use.

This study introduces a novel approach to utilizing CPW as a biosorbent to remove RB without chemical modification or carbonization. Unlike previous studies that focused on modified or treated adsorbents, this study proves that CPW in its natural form remains high and has a competitive adsorption capacity as a biosorbent, making it a more sustainable, economical and easy-to-apply alternative. Through a thorough analysis of kinetics, isotherms and thermodynamics, this study provides an in-depth understanding of the adsorption mechanism and optimal conditions for removing RB dye from wastewater. Furthermore, this research addresses two major environmental challenges: transforming abundant agricultural waste, such as coffee peel, into an efficient biosorbent and applying the adsorption process as an effective method in industrial wastewater treatment.

Table 1. Chemical Composition of Coffee Peel

Component	Amount (% weight)
Cellulose	39.2 ± 0.2
Hemicellulose	12.6 ± 0.1
Klason Lignin	23.3 ± 0.1
Acid-soluble lignin	2.9 ± 0.4
Extractive	8.7 ± 0.2
Ash	9.5 ± 0.2

2. EXPERIMENTAL SECTION

2.1 Materials and Instruments

CPW was obtained from Bengkalis City, Indonesia. The chemicals utilized in this study were Rhodamine B ($C_{28}H_{31}N_2O_3Cl$), citric acid ($C_6H_8O_7$), nitric acid (HNO_3), sodium hydroxide (NaOH), potassium chloride (KCl), buffer solution, distilled water, and filter paper. All chemicals were of analytical grade and produced by Merck.

This study also used various laboratory tools and instruments such as the necessary glassware, analytical balance (Kern & Sohn GmbH), shaker (Edmund Bühler 7400 Tubingen), pH meter (Metrohm), oven (Memmert), sieve (Fritsch, Germany), FTIR (IRTracer-100, Shimadzu), Spektrofotometer UV-Vis (Genesys 1280 dengan Nomor Seri A120657), and SEM-EDX (Hitachi FLEXSEM 1000).

2.2 Methods

2.2.1 Preparation and Characterization of CPW

CPW was first washed and subsequently air-dried at a stable room temperature. After drying, the CPW was finely ground into a powder and screened to gain a particle size of 36 μm. The obtained CPW powder was subsequently immersed in a 0.01 M HNO_3 solution with a specific solid-to-liquid (S/L) ratio of 1:5 for 3 hours. Subsequently, distilled water was utilized to rinse the sample until the pH reached a neutral level, followed by filtration and air drying (Hevira et al., 2021). CPW was subjected to FTIR and SEM-EDX analysis prior to and following RB adsorption to assess its functional groups and surface morphology.

2.2.2 pHpzc Determination

A total of 0.1 g of CPW biosorbent was put into 8 Erlenmeyer flasks, each added with 50 mL of 0.1 M KCl solution with an initial pH variation in the range of 2–9, which was adjusted utilizing 0.01 M NaOH and 0.01 M HNO_3. For 24 hours, the solution was continuously stirred using a shaker, the final pH of each sample was recorded, and the initial pH versus △pH (final pH – initial pH) data were plotted on a graph. The point where the curve intersects at zero indicates the pHpzc value (Zein et al., 2022).

2.2.3 Batch Adsorption Study

The batch adsorption tests involved the addition of 0.1 g of CPW powder to an erlenmeyer flask containing 25 mL of RB solution. The mixture was agitated using a shaker set at a continuous speed of 100 rpm for 60 minutes. A comprehensive evaluation of the adsorption process was performed to examine the influence of pH variation (5–11), initial RB concentration (100–1400 mg/L), and contact duration (15–120 minutes). The final RB at a maximum (max) wavelength of 554 nm. RB adsorbed amounts were derived utilizing Equations (1) and (2).

$$q_e = \frac{(C_0 - C_e)}{m} \times V \tag{1}$$

$$\%R = \frac{(C_0 - C_e)}{C_0} \times 100 \tag{2}$$

Within this equation, q_e represents the adsorption capacity (mg/g), C_0 represents the initial concentration of the adsorbate (mg/L), while C_e denotes the equilibrium concentration (mg/L). Additionally, mmm corresponds to the mass of the biosorbent (g), and V indicates the total volume of the solution (L) and %R is the percentage of adsorption (%) (Hevira et al., 2021).

2.2.4 Thermodynamic Study

10 mL of RB solution and 0.1 g of biosorbent were added to 15 Erlenmeyer flasks containing concentrations of 10, 20,

30, 40, and 50 mg/L in different amounts at the previously determined optimum pH and contact time. The solution temperature was varied at 25 K, 35 K, and 45 K, and the mixtures were stirred at a constant speed of 100 rpm. Following the adsorption procedure, the solutions underwent filtration and the filtrates were measured by a UV-Vis a spectrophotometer operating at an optimal wavelength of 554 nm (Hevira et al., 2021)

3. RESULTS AND DISCUSSION

3.1 FTIR Analysis

FTIR analysis was conducted to identify functional groups found in CPW. The FTIR spectra was analyzed on CPW before and after RB adsorption process covering wavenumbers between 4000 and 500 cm^{-1}, as shown in Figure 1. The peak at 3272.97 cm^{-1} indicates O−H vibrational stretching originating from hemicellulose, cellulose, and lignin. In addition, the peak at 2923.95 cm^{-1} indicates aliphatic C−H stretching vibrations, which are also related to the structure of hemicellulose, cellulose, and lignin (Dung et al., 2023). Functional groups responsible for RB adsorption were also identified on the biosorbent surface through FTIR spectral analysis, as summarized in Table 2.

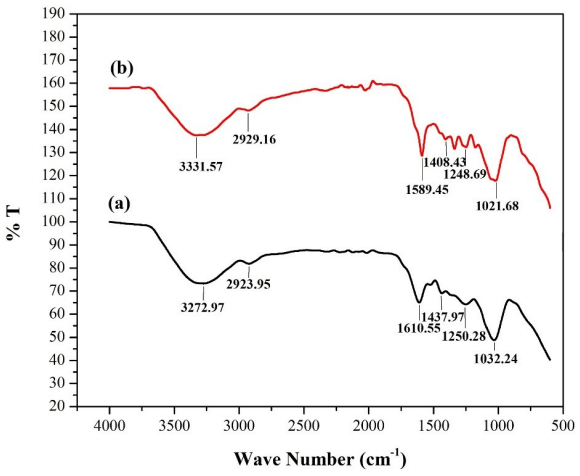

Figure 1. The FTIR Spectra of CPW Before (a) and After Adsorption (b)

After the adsorption of RB, notable alterations in the position of peaks and reductions in intensity were observed in the FTIR spectra, pointing to strong interactions between CPW and the dye molecules. The overall decline in peak intensity suggests that several functional groups actively participated in the adsorption process, reducing their free vibrational modes. The O−H stretching peak, initially at 3272.97 cm^{-1}, shifted to 3331.57 cm^{-1}, accompanied by a reduction in intensity. This shift points to the establishment of hydrogen bonding between hydroxyl groups in CPW and RB molecules (Mansour et al., 2022). Likewise, the C=C stretching peak moved from 1610.55 cm^{-1} to 1589.45 cm^{-1}, with decreased intensity, indicating π-π stacking interactions. Additionally, the C−O stretching peaks experienced shifts from 1250.28 cm^{-1} to 1248.69 cm^{-1} and from 1032.24 cm^{-1} to 1021.68 cm^{-1}, both showing intensity reductions. This points to electrostatic interactions as a key factor in binding RB to oxygen-containing groups in CPW. These peak shifts and intensity decreases confirmed that hydrogen bonding, interactions via electrostatics, and π-π stacking mechanisms were responsible for RB adsorption onto CPW (Wierzbicka et al., 2022).

3.2 SEM – EDX Analysis

The SEM examination presented in Figure 2 illustrates the alterations in the surface morphology of CPW prior to and following RB adsorption. Before adsorption, the surface of the biosorbent exhibits a rough, irregular, and porous texture. However, after absorption, the closed pores become more densely filled with dye, leading to a smoother surface. This change indicates that RB molecules have been adsorbed and have covered the surface of the biosorbent (Dai et al., 2021; Ramadhani et al., 2020). The smooth and even surface after the absorption process suggests the formation of a monolayer resulting from the uniform binding of dye molecules to the biosorbent's surface (Bhatti et al., 2020). Additionally, structural changes in the biosorbent may occur due to chemical interactions between RB and the pore walls. This interaction could lead to pore reorganization, further confirming the adsorption mechanism (Kyriakopoulos et al., 2024).

Table 3 shows alterations in elemental composition of the biosorbent before and after adsorption. The CPW biosorbent predominantly comprises carbon (C) and oxygen (O) elements. CPW is an organic material rich in both carbon and oxygen elements. After RB adsorption, there is a rise in carbon and a fall in oxygen levels. This increase in carbon indicates the accumulation of RB molecules, which are also rich in carbon. Meanwhile, the decrease in oxygen is believed to result from the interaction of RB with active sites containing oxygen, leading to a relative reduction in the oxygen content (Zein et al., 2022).

3.3 pHpzc Analysis

pH point of zero charge (pHpzc) is characterised as the pH where the surface of a material exhibits a neutral state without any electrical charge. This parameter plays an important role in adsorption research because it affects the surface charge properties of the adsorbent under various pH conditions (Putri et al., 2024). As shown in Figure 3, the pHpzc value for CPW biosorbent is 7.009. Under pH conditions below the pHpzc, the biosorbent surface exhibits a positive charge, increasing its likelihood of anion binding. Conversely, when the pH is above the pHpzc, The surface is rendered negatively charged, making it more effective

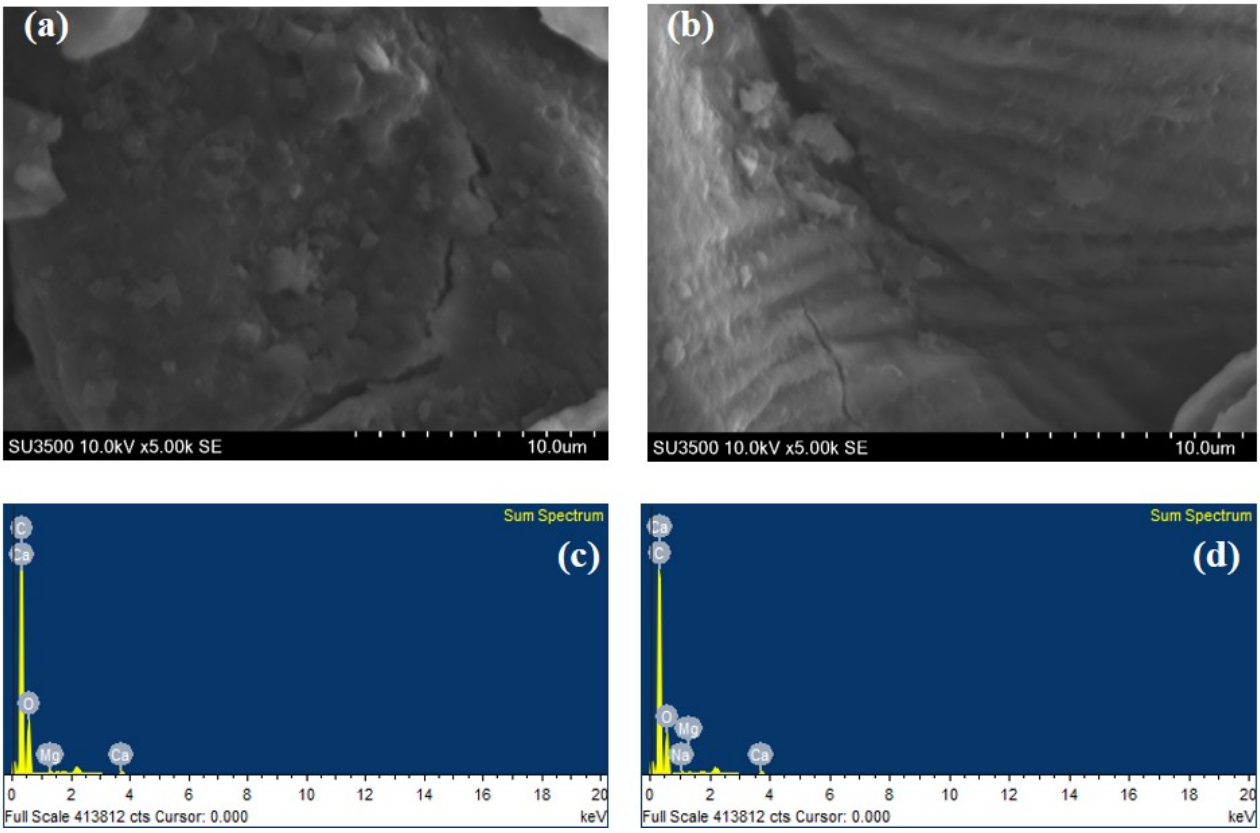

Figure 2. SEM Images of CPW Before (a) and After Adsorption (b). EDX Graph Before (c) and After Adsorption (d)

Table 2. Wave Number Shift Values in the FTIR Spectrum of CPW Before and After RB Adsorption

Before Adsorption (cm^{-1})	%T	After adsorption (cm^{-1})	%T	Functional group
3272.97	73.28	3331.57	79.56	O−H
2923.95	81.85	2929.16	90.30	C−H
1610.55	65.07	1589.45	70.77	C=C
1437.97	68.59	1408.43	77.84	C−H
1250.28	64.29	1248.69	74.46	C−O
1032.24	48.80	1021.68	59.92	C−O

Table 3. Changes in CPW's Chemical Composition at Specific Sites Following Adsorption

Element	Relative abundance of element	
	Before Adsorption (% Wt)	After Adsorption (% Wt)
C	65.08	67.37
O	34.02	31.14
Mg	0.12	0.13
Ca	1.05	0.78
Na	-	0.31

at attracting cations (Jamali and Akbari, 2021). Understanding the pHpzc aids in hypothesizing Functional groups' ionisation behaviour and how they interact with adsorbates in solutions. It also helps predict the pH range where adsorption capacity is maximized (Zein et al., 2022).

Table 4. Adsorption Isotherm Parameters

Langmuir				Freundlich		
R^2	q_m (mg/g)	K_L (L/mg)	R_L	R^2	K_F ((L/mg)$^{1/n}$)	1/n
0.9945	65.7895	0.0397	0.0206 0.2014	0.8882	7.9561	0.367

Table 5. Adsorption Kinetic Parameters

Pseudo-First-Order			Pseudo-Second-Order		
R^2	k_1 (min^{-1})	q_e (Calc) (mg/g)	R^2	k_2 (g/mg.min)	q_e (Calc) (mg/g)
0.3956	0.0165	12.4547	0.9942	0.0039	70.4225

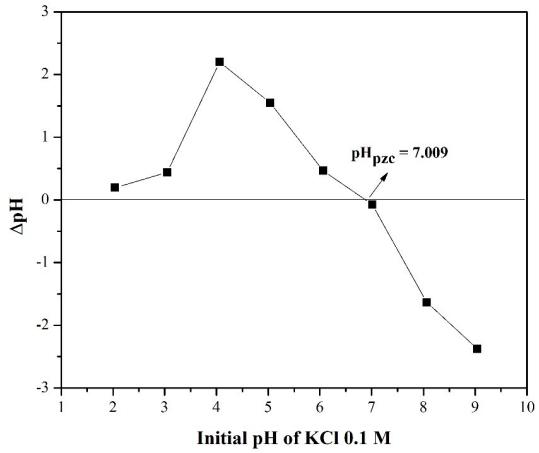

Figure 3. pHpzc for CPW

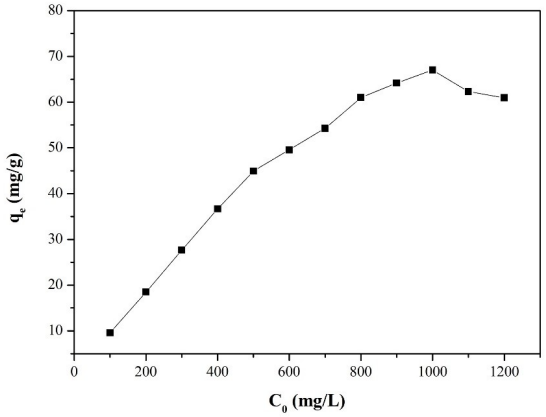

Figure 5. Effect of Initial Concentration of RB on Adsorption Capacity

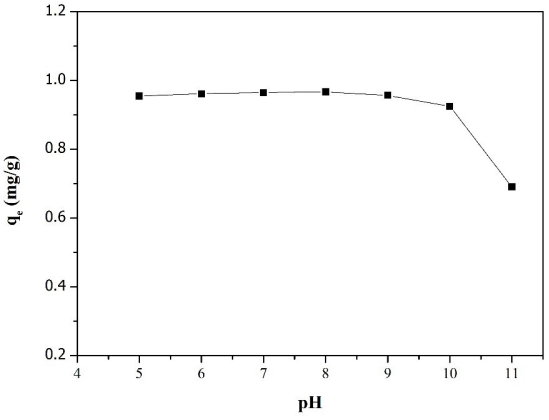

Figure 4. Effect of pH on the Adsorption Capacity of RB

3.4 Effect of pH

The effect of solution pH on the adsorption of RB was investigated based on the results of the pHpzc for CPW. This study focused on a pH range from 5 to 11. As illustrated in Figure 4, the adsorption capacity demonstrated an increasing pattern with rising pH levels, attaining its peak performance at pH 8 with a max. adsorption capacity of 0.9667 mg/g. At the appropriate pH, positively charged RB exhibits electrostatic interactions with the negatively charged biosorbent surface. At reduced pH values, the biosorbent surface often acquires a positive charge due to the presence of H^+ ions, resulting in electrostatic repulsion that reduces the adsorption capacity. H^+ ions compete with RB for surface active sites and reduce adsorption efficiency. H^+ will dominate the binding sites, preventing RB from interacting with the biosorbent surface. As the pH increases, the number of H^+ ions in the solution decreases, and the biosorbent surface begins to deprotonate, producing a negative charge that further enhances the electrostatic interaction between the biosorbent surface and RB. However, the adsorption capacity decreases above the optimum pH because the biosorbent surface becomes oversaturated with negative charges, weakening the electrostatic attraction to RB. In addition, at high

Table 6. Thermodynamic Parameters of Adsorption

Temperature (K)	ΔG° (kJ/mol)	ΔH° (kJ/mol)	ΔS° (kJ/mol.K)
298	-1.0010		
308	-1.1347	-0.6408	0.0013
318	-1.0278		

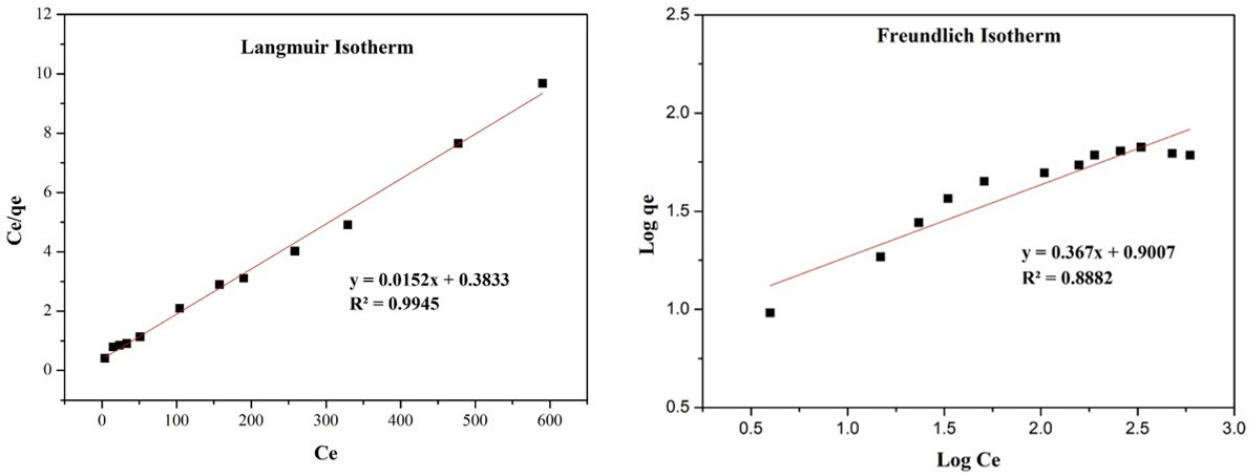

Figure 6. Langmuir and Freundlich Isotherm raphs

pH, RB may undergo chemical changes or precipitation that can also reduce adsorption efficiency RB may undergo chemical changes or precipitation that can also reduce adsorption efficiency (Dilekoğlu, 2022; Jin et al., 2019).

The analysis of pH influence on dye adsorption has shown that highest possible adsorption occurs at pH levels more significantly than the point of zero charge (pHpzc). This indicates that RB adsorption is more efficient under basic conditions, primarily due to the biosorbent's negatively charged surface and the positively charged RB molecule's electrostatic contact.

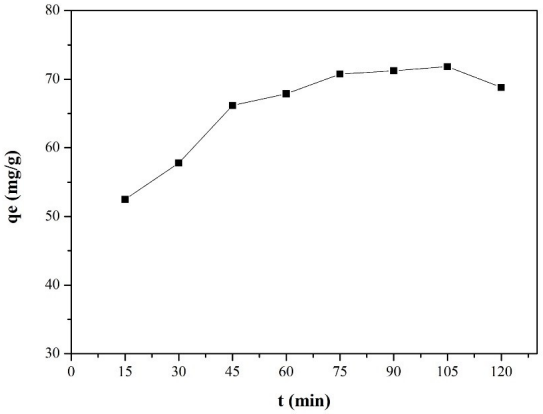

Figure 7. Effect of Contact Time On Adsorption Capacity

3.5 Effect of Initial Dye Concentration and Isotherm Study

Figure 5 illustrates that the adsorption capacity increases with higher concentrations of RB until it reaches an optimal point at 1000 mg/L, where 67.0418 mg/g is the adsorption capability. Generally, an increase in the dye removal rate correlates with a greater driving force that helps transcend the resistance to translocation of adsorbate molecules from the bulk solution onto the biosorbent surface through mass transfer mechanisms (Dai et al., 2021). As RB levels change rises, As the concentration of dye molecules in the solution escalates, the probability of molecular interactions with the biosorbent surface intensifies, resulting in more frequent collisions (Musafira et al., 2019). This rise in adsorption capacity indicates that more RB molecules are binding to the areas of activity on the surface of the biosorbent. As RB levels change is high, free active sites are still available, facilitating increased adsorption on the biosorbent surface (Bilal et al., 2018). However, beyond the optimal concentration, the adsorption capacity decreases. This decline occurs because the active sites on the biosorbent surface become saturated with RB molecules, preventing the effective adsorption of additional dye molecules (Dai et al., 2021).

The Langmuir and Freundlich models utilized in this study are the adsorption isotherm models. The Langmuir isotherm describes the adsorption process occurring on the surface of a homogeneous biosorbent, yielding the formation of a single layer (monolayer). In contrast, the Freundlich isotherm accounts for adsorption in multiple layers (multi-

Table 7. Contrasting the RB adsorption Efficiency of CPW with Different Adsorbents

Adsorbent	q_m (mg/g)	References
Garlic peel	3.5	(Zhao et al., 2019)
Garlic peel modified with citric acid	6.3	(Zhao et al., 2019)
Cypress/False Cypress Fruit	6.83	(Gul et al., 2022)
Almond shell	14.7	(Senol et al., 2023)
Pomegranate peel	30.47	(Ghibate et al., 2021)
Tapioca peel waste	33.10	(Vigneshwaran et al., 2021)
Paspalum notatum grass waste	54	(Zahir et al., 2020)
Paspalum notatum grass waste modified with hydrochloric acid	72.4	(Zahir et al., 2020)
Rosemary waste (activated carbon)	65.78	(Naboulsi et al., 2023)
Coffee peel waste	71.84	This research

layer) on a heterogeneous surface Kurniawati et al. (2023); Ramadhani et al. (2020). As shown in Figure 6, the Langmuir isotherm accurately captures the adsorption mechanism of RB using CPW as a biosorbent. This conclusion is supported by the R^2 value, close to 1, precisely 0.9945. The parameters obtained from both isotherm models are presented in Table 4.

3.6 Effect of Contact Time and Kinetic Study

Figure 7 shows that the max. adsorption capacity was achieved at a contact time of 105 minutes with a 71.8454 mg/g value. The longer the contact time, the more adsorption capacity increases (Guiza, 2017). This enhancement is attributed to the lengthened collision phase between the CPW and the dye molecules, which increases the likelihood of dye adsorption by the CPW. In the early stages, the CPW surface retains a high number of active sites (Ramadhani et al., 2020). However, if the contact time is extended too long, the adsorption capacity may decrease. The active sites bound to RB molecules become saturated and has reached its saturation point for molecule binding (Peng et al., 2018).

Contact time's effect on adsorption capacity was analyzed to establish the appropriate adsorption kinetic model. Kinetic analysis was performed to gain shedding light on the adsorption behavior and mass transfer processes. The contact time data were evaluated utilizing pseudo-second-order kinetic models and pseudo-first-order, as visualized in Figure 8, and Table 5 compiles the relevant parameters.

The adsorption process of RB adsorption utilises a kinetic model that is pseudo-second order, as evidenced by the R^2 value, which is closer to 1 compared to that of the pseudo-first-order model. Moreover, the calculated adsorption capacity of RB based on the pseudo-second-order model (qe calc) closely matches the experimental adsorption capacity value (qe) These findings suggest that the adsorption of RB by CPW involves chemical interactions or chemisorption, further supported by its alignment with the Langmuir isotherm model (Matias et al., 2020). Additionally, other studies have found that the adsorption process of RB using *Raphia hookerie* fruit epicarp Inyinbor et al. (2016) and pomegranate peel Ghibate et al. (2021) also follows a pseudo-second-order kinetic model.

3.7 Thermodynamics Study

Table 6 shows that the Gibbs free energy change ($\triangle G^\circ$) for CPW biosorbent is negative, demonstrating that the adsorption process happens on its own. The standard enthalpy change ($\triangle H^\circ$) is also negative, proving the exothermic nature of the adsorption process (releasing heat). A Similar result was found in a study using activated banana peel carbon as an adsorbent for RB adsorption (Singh et al., 2020). Meanwhile, the positive standard entropy change ($\triangle S^\circ$) indicates an increase in disorder at the solid-liquid contact surface during RB adsorption process. This increase in disorder is caused by water molecules that are replaced during the adsorption process, where the water molecules have a higher translational entropy than the adsorbed dye molecules. This increases the overall disorder of the system (Ali et al., 2022; Naboulsi et al., 2023).

3.8 Comparison of CPW Adsorption Capacity with Another Biomass

Table 7 shows that compared to other adsorbents, CPW demonstrates superior adsorption capacity and almost the same as that of Paspalum notatum grass waste modified with hydrochloric acid biosorbent. This proves that CPW has good adsorption capacity. Ease of sample preparation and lack of precursors are additional advantages of biowaste as a biosorbent. The plentiful availability of biowaste in nature presents both an solution and opportunity for managing agricultural waste. It has broad potential as a biosorbent in synthetic dye wastewater. Using adsorbents without modification and carbonization has been proven to adsorb RB dyes, making it a novelty in this study. Therefore, using CPW to remove dye from wastewater meets the zero-waste adsorption concept, offering an effective and cost-efficient technology.

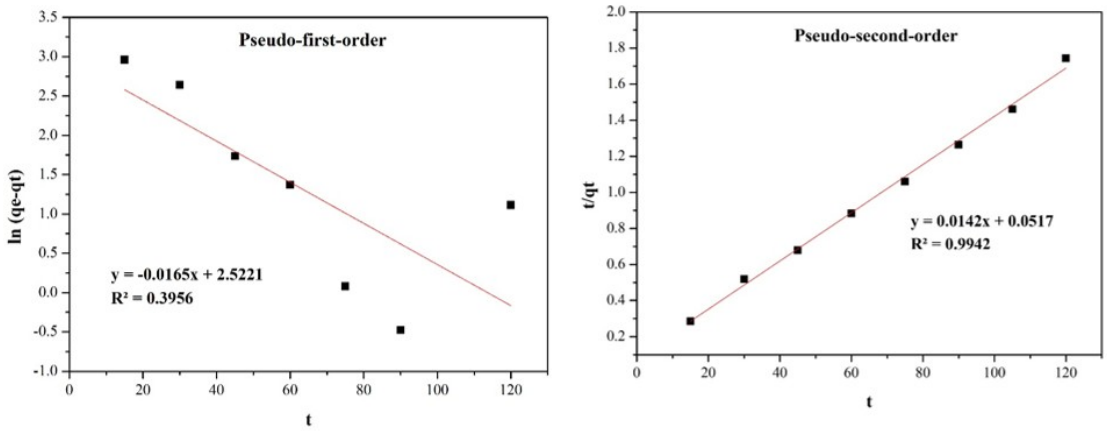

Figure 8. Adsorption Kinetic Model Graph

4. CONCLUSIONS

This research underscores the remarkable efficacy of CPW as an environmentally sustainable biosorbent for RB elimination from wastewater, under the adjusted conditions of pH 8, an initial concentration of adsorbate at 1000 mg/L was used, with a contact duration of 105 minutes, the adsorption process reached its max. capacity of 71.8454 mg/g. Isotherm analysis confirmed that the adsorption mechanism follows the Langmuir model, indicating monolayer on a homogeneously structured adsorbent surface. Furthermore, the adsorption kinetics exhibited conformity with the pseudo-second-order model, signifying the dominance of chemisorption in the process of chemisorption as the primary mechanism. Thermodynamic analysis further supports this, showing that the process occurs spontaneously and releases heat, characteristic of chemisorption. FTIR characterization validated the presence and role of functional groups like -OH and C=O in the adsorption mechanism. This study provides a scientific basis for utilizing CPW as a sustainable solution in dye wastewater treatment. Further development is needed to test the efficiency on an industrial scale and assess the regeneration process of the biosorbent.

5. ACKNOWLEDGEMENT

The authors extend their gratitude to the Department of Chemistry, Andalas University, for supporting the laboratory facilities provided during this research. They also express their appreciation to the reviewers for their valuable input and comments, which have helped improve the quality of this article.

REFERENCES

Al-Kahtani, A. A. (2017). Photocatalytic Degradation of Rhodamine B Dye in Wastewater Using Gelatin/CuS/PVA Nanocomposites under Solar Light Irradiation. *Journal of Biomaterials and Nanobiotechnology*, **8**(1); 66–82

Al-Tohamy, R., S. S. Ali, F. Li, K. M. Okasha, Y. A. G. Mahmoud, T. Elsamahy, H. Jiao, Y. Fu, and J. Sun (2022). A Critical Review on the Treatment of Dye-Containing Wastewater: Ecotoxicological and Health Concerns of Textile Dyes and Possible Remediation Approaches for Environmental Safety. *Ecotoxicology and Environmental Safety*, **231**; 113160

Ali, N. S., N. M. Jabbar, S. M. Alardhi, H. S. Majdi, and T. M. Albayati (2022). Adsorption of Methyl Violet Dye Onto a Prepared Bio-Adsorbent from Date Seeds: Isotherm, Kinetics, and Thermodynamic Studies. *Heliyon*, **8**(8); e10276

Amalina, F., A. S. Abd Razak, S. Krishnan, A. W. Zularisam, and M. Nasrullah (2022). A Review of Eco-Sustainable Techniques for the Removal of Rhodamine B Dye Utilizing Biomass Residue Adsorbents. *Physics and Chemistry of the Earth*, **128**; 103267

Bhatti, H. N., Y. Safa, S. M. Yakout, O. H. Shair, M. Iqbal, and A. Nazir (2020). Efficient Removal of Dyes Using Carboxymethyl Cellulose/Alginate/Polyvinyl Alcohol/Rice Husk Composite: Adsorption/Desorption, Kinetics and Recycling Studies. *International Journal of Biological Macromolecules*, **150**; 861–870

Bilal, M., T. Rasheed, J. E. Sosa-Hernández, A. Raza, F. Nabeel, and H. M. N. Iqbal (2018). Biosorption: An Interplay Between Marine Algae and Potentially Toxic Elements—A Review. *Marine Drugs*, **16**; 65

Cheruiyot, G. K., W. C. Wanyonyi, J. J. Kiplimo, and E. N. Maina (2019). Adsorption of Toxic Crystal Violet Dye Using Coffee Husks: Equilibrium, Kinetics and Thermodynamics Study. *Scientific African*, **5**; e00116

Dai, J., Z. Ye, K. Jin, L. Zhang, H. Han, and R. Sha (2021). Modified Garlic Straws as New Adsorbents for Removing Ionic Dyes from Aqueous Solutions. *Desalination and Water Treatment*, **237**; 259–270

Dilekoğlu, M. F. (2022). Malachite Green Adsorption from Aqueous Solutions Onto Biochar Derived from Sheep Ma-

nure: Adsorption Kinetics, Isotherm, Thermodynamic, and Mechanism. *International Journal of Phytoremediation*, **24**(4); 436–446

Dung, V. N., T. T. D. Cham, N. M. V. Chau, M. N. Hung, T. P. Tuyet, M. T. T. Tuyet, and Q. N. Long (2023). Data on Chemical Composition of Coffee Husks and Lignin Microparticles as Their Extracted Product. *Data in Brief*, **51**; 109781

Ghibate, R., O. Senhaji, and R. Taouil (2021). Kinetic and Thermodynamic Approaches on Rhodamine B Adsorption Onto Pomegranate Peel. *Case Studies in Chemical and Environmental Engineering*, **3**; 100078

Guiza, S. (2017). Biosorption of Heavy Metal from Aqueous Solution Using Cellulosic Waste Orange Peel. *Ecological Engineering*, **99**; 134–140

Gul, S., H. Gul, M. Gul, R. Khattak, G. Rukh, M. S. Khan, and H. A. Aouissi (2022). Enhanced Adsorption of Rhodamine B on Biomass of Cypress/False Cypress (*Chamaecyparis lawsoniana*) Fruit: Optimization and Kinetic Study. *Water (Switzerland)*, **14**(19); 2987

Harrache, Z., M. Abbas, T. Aksil, and M. Trari (2019). Thermodynamic and Kinetics Studies on Adsorption of Indigo Carmine from Aqueous Solution by Activated Carbon. *Microchemical Journal*, **144**; 180–189

Hevira, L., Zilfa, Rahmayeni, J. O. Ighalo, H. Aziz, and R. Zein (2021). *Terminalia Catappa* Shell as Low-Cost Biosorbent for the Removal of Methylene Blue from Aqueous Solutions. *Journal of Industrial and Engineering Chemistry*, **97**; 188–199

International Agency for Research on Cancer (2022). *Agents Classified by the IARC Monographs*. Igarss

Inyinbor, A. A., F. A. Adekola, and G. A. Olatunji (2016). Kinetics, Isotherms and Thermodynamic Modeling of Liquid Phase Adsorption of Rhodamine B Dye Onto *Raphia Hookerie* Fruit Epicarp. *Water Resources and Industry*, **15**; 14–27

Jamali, M. and A. Akbari (2021). Facile Fabrication of Magnetic Chitosan Hydrogel Beads and Modified by Interfacial Polymerization Method and Study of Adsorption of Cationic/Anionic Dyes from Aqueous Solution. *Journal of Environmental Chemical Engineering*, **9**(3); 105175

Jin, Y., C. Zeng, Q. F. Lü, and Y. Yu (2019). Efficient Adsorption of Methylene Blue and Lead Ions in Aqueous Solutions by 5-Sulfosalicylic Acid Modified Lignin. *International Journal of Biological Macromolecules*, **123**; 50–58

Juwita, A. I., A. Mustafa, and R. Tamrin (2017). Studi Pemanfaatan Kulit Kopi Arabika (*Coffee Arabica L.*) sebagai Mikro Organisme Lokal (MOL). *AGROINTEK*, **11**(1); 1–8

Kurniawati, D., Y. Prestica, S. Sy, and N. L. Pernadi (2023). Methylene Blue Adsorption by Langsat Peel (*Lansium Domesticum*) Waste. *Jurnal Litbang Industri*, **13**(2); 93–98

Kyriakopoulos, G. L., K. Tsimnadis, I. Sebos, and Y. Charabi (2024). Investigating the Effect of Pore Size Distribution on the Sorption Types and the Adsorption-Deformation Characteristics of Porous Continua: The Case of Adsorption on Carbonaceous Materials. *Crystals*, **14**(8); 742

Mansour, A. T., A. E. Alprol, K. M. Abualnaja, H. S. El-Beltagi, K. M. A. Ramadan, and M. Ashour (2022). Dried Brown Seaweed's Phytoremediation Potential for Methylene Blue Dye Removal from Aquatic Environments. *Polymers*, **14**(7); 1375

Matias, C. A., L. J. Guisolphi Gomes De Oliveira, R. Geremias, and J. Stolberg (2020). Biosorption of Rhodamine B from Aqueous Solution Using *Araucaria Angustifolia* Sterile Bracts. *Revista Internacional de Contaminacion Ambiental*, **36**(1); 97–104

Musafira, M., N. M. Adam, and D. J. Puspitasari (2019). Pemanfaatan Limbah Kulit Buah Pisang Kepok (*Musa Paradisiaca*) sebagai Biosorben Zat Warna Rhodamin B. *Kovalen: Jurnal Riset Kimia*, **5**(3); 308–314

Naboulsi, A., I. Naboulsi, A. Regti, M. El Himri, and M. El Haddad (2023). The Valorization of Rosemary Waste as A New Biosorbent to Eliminate the Rhodamine B Dye. *Microchemical Journal*, **191**; 108790

Palapa, N. R., A. Amri, and Y. Hanifah (2023). Potential Indonesian Rice Husk for Wastewater Treatment Agricultural Waste Preparation and Dye Removal Application. *Indonesian Journal of Environmental Management and Sustainability*, **7**(4); 160–165

Peng, S. H., R. Wang, L. Z. Yang, L. He, X. He, and X. Liu (2018). Biosorption of Copper, Zinc, Cadmium and Chromium Ions From Aqueous Solution by Natural Foxtail Millet Shell. *Ecotoxicology and Environmental Safety*, **165**; 61–69

Putri, B. I., F. S. Arsyad, and A. Lesbani (2024). Hydrothermal Carbonization of *Eucheuma cottonii* for Selective Adsorption of Anionic Dyes. *Indonesian Journal of Environmental Management and Sustainability*, **8**(4); 154–165

Ramadhani, P., Z. Chaidir, Zilfa, Z. B. Tomi, D. Rahmiarti, and R. Zein (2020). Shrimp Shell (*Metapenaeus Monoceros*) Waste as A Low-Cost Adsorbent for Metanil Yellow Dye Removal in Aqueous Solution. *Desalination and Water Treatment*, **197**; 413–423

Rangabhashiyam, S., N. Anu, and N. Selvaraju (2013). Sequestration of Dye from Textile Industry Wastewater using Agricultural Waste Products as Adsorbents. *Journal of Environmental Chemical Engineering*, **1**(4); 629–641

Senol, Z. M., N. E. Messaoudi, Y. Fernine, and Z. S. Keskin (2023). Bioremoval of Rhodamine B Dye from Aqueous Solution by using Agricultural Solid Waste (Almond Shell): Experimental and DFT Modeling Studies. *Biomass Conversion and Biorefinery*, **14**; 17927–17940

Singh, S., A. Kumar, and H. Gupta (2020). Activated Banana Peel Carbon: A Potential Adsorbent for Rhodamine B Decontamination from Aqueous System. *Applied Water*

Science, **10**; 185

Subramaniam, R. and S. Kumar Ponnusamy (2015). Novel Adsorbent from Agricultural Waste (Cashew Nut Shell) for Methylene Blue Dye Removal: Optimization by Response Surface Methodology. *Water Resources and Industry*, **11**; 64–70

Vigneshwaran, S., P. Sirajudheen, P. Karthikeyan, and S. Meenakshi (2021). Fabrication of Sulfur-Doped Biochar Derived from Tapioca Peel Waste with Superior Adsorption Performance for the Removal of Malachite Green and Rhodamine B Dyes. *Surfaces and Interfaces*, **23**; 100920

Wierzbicka, E., . Kusmierek, A. Swiatkowski, and I. Legocka (2022). Efficient Rhodamine B Dye Removal from Water by Acid- and Organo-Modified Halloysites. *Minerals*, **12**(3); 350

Zahir, A., Z. Aslam, U. Aslam, A. Abdullah, R. Ali, and M. M. Bello (2020). *Paspalum Notatum* Grass-Waste-Based Adsorbent for Rhodamine B Removal from Polluted Water. *Chemical and Biochemical Engineering Quarterly*, **34**(2); 93–104

Zein, R., J. S. Purnomo, P. Ramadhani, M. F. Alif, and S. Safni (2022). Lemongrass (*Cymbopogon Nardus*) Leaves Biowaste as An Effective and Low-Cost Adsorbent for Methylene Blue Dyes Removal: Isotherms, Kinetics, and Thermodynamics Studies. *Separation Science and Technology*, **57**(15); 2341–2357

Zhao, Y., L. Zhu, W. Li, J. Liu, X. Liu, and K. Huang (2019). Insights Into Enhanced Adsorptive Removal of Rhodamine B by Different Chemically Modified Garlic Peels: Comparison, Kinetics, Isotherms, Thermodynamics and Mechanism. *Journal of Molecular Liquids*, **293**; 111516

